

Boundary Layer Control with Atmospheric Plasma Discharges

Gabriel I. Font*

US Air Force Academy, CO, 80840

Recent studies have investigated the use of plasma actuators for the active control of the boundary layer on turbine blades. While the overall effects have been quantified through experiments, the exact nature of the plasma and its momentum transfer mechanisms have not been well characterized. In this study, particle-in-cell and Monte-Carlo (PIC-DSMC) methods are used to computationally explore the plasma discharge and its interaction with the flow. The plasma composition, its methods of momentum addition, and the physics of its generation are quantified. Comparisons with experiments are made in order to support the findings. Simulations indicate that the plasma is generated through an electron avalanche in a dielectric barrier discharge. The plasma is created as the electrons stream to the dielectric on the first half of the electrode bias cycle and stream back on the second half. Momentum is imparted to the flow on both half cycles but the ionization is not equal during both half cycles. This results in the plasma actuator producing a net force in one direction.

I. Introduction

THE lift performance of an airfoil, as the angle of attack increases, is limited by the ability to maintain the boundary layer attachment to the suction surface. When the chordwise pressure gradient becomes sufficiently large, the boundary layer loses its momentum and separates from the surface. Traditionally, vortex generators or pneumatic jets have been used to reenergize the boundary layer and promote attachment. A recently developed alternative utilizes a plasma to impart momentum to the boundary layer for the same result.¹⁻⁶ It has been successfully employed for boundary layer separation control in airfoils and turbine blades.²⁻⁵ It is called a plasma actuator and is effective in increasing lift and lowering drag.⁴ The method consists of generating a plasma (ionized gas) in the boundary layer which is in danger of separation. The ions and electrons accelerate in the electric field used to generate the plasma and then impart their momentum to the air molecules through collisions. The plasma, therefore, acts as a momentum source to the boundary layer allowing it to remain attached throughout a larger portion of the airfoil.

The plasma actuator consists of two long conducting (metal) strips placed parallel to each other. (see Fig. 1) The two strips act as electrodes and are arranged with a horizontal offset from each other. The lower electrode is covered with a dielectric while the upper electrode is exposed to the flow. An alternating voltage is applied across the electrodes resulting in the generation of plasma in the vicinity of the electrodes. The voltage difference applied between the electrodes can vary from 1 kV to as high as 5 kV. The frequency of the driving voltage is typically from 1 to 10 kHz.

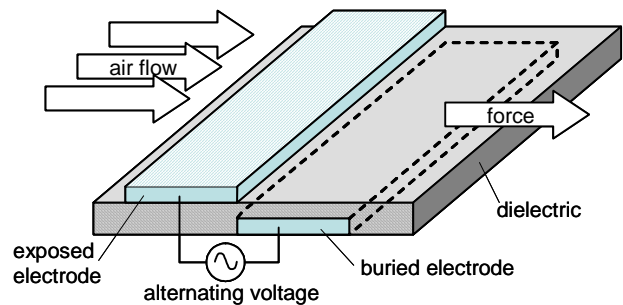


Figure 1. Plasma actuator configuration.

* Professor, Department of Physics, AIAA Member.

This paper is declared a work of the U.S. Government and is not subject to copyright protection in the United States.

The creation of the plasma may be due to one of two mechanisms. The first mechanism may be capacitive coupling⁷, where the electrons in the plasma gain energy by oscillating in the fluctuating electric fields in the sheaths. The sheaths can be thought of as electrical boundary layers that are created near surfaces due to the difference in the thermal velocities of the ions and the electrons. A capacitively coupled plasma is typically characterized by a spatially diffuse glow that persists uniformly in time over the multiple electrode bias cycles. This type of plasma is often used for materials processing at pressures of 1-10 Torr (0.001-0.01 atm).

The second mechanism is an electron avalanche. In this mechanism, the electrons accelerate in an electric field and gain sufficient energy to cause ionization when they collide with the neutrals. The newly created electrons then accelerate in the field and cause further ionization. The result is a run-away cascade of ionization events. This type of plasma persists over a short time (nano-seconds) and is concentrated in a small space (fractions of millimeters). If this plasma is initiated with a broad electrode, millions of individual cascade events may combine to form what appears to be a uniform plasma. Experimental measurements taken with sufficient time resolution, however, will still reveal the individual electron avalanche events.⁸⁻¹¹ This type of plasma is typically used for materials processing at atmospheric pressures.⁷

Current measurements taken by Enloe, et al.⁶ (reproduced in Fig. 2) reveal individual current spikes at time scales which are more than 100 times faster than the electrode bias cycle. This is indicative of electron avalanches and not a capacitively coupled plasma, where the current measurements would follow the bias cycle. The plasma is also observed to extinguish (cease to exist) between each half of the bias cycle. This suggests that the plasma is regenerated by the electric field each time it changes direction. These two observations lead to the conclusion that the plasma actuator is working to generate plasma through electron avalanches. When the upper electrode is biased negatively, the electrons avalanche toward the buried electrode. Because the buried electrode is covered with a dielectric, the electrons are stopped from leaving and remain on the surface of the dielectric resulting in the extinguishing

of the plasma. When the electric field reverses on the latter half of the bias cycle, the electrons are again accelerated (this time toward the exposed electrode) and regenerate the plasma through a second avalanche. This type of plasma discharge is commonly known as a dielectric barrier discharge (DBD).

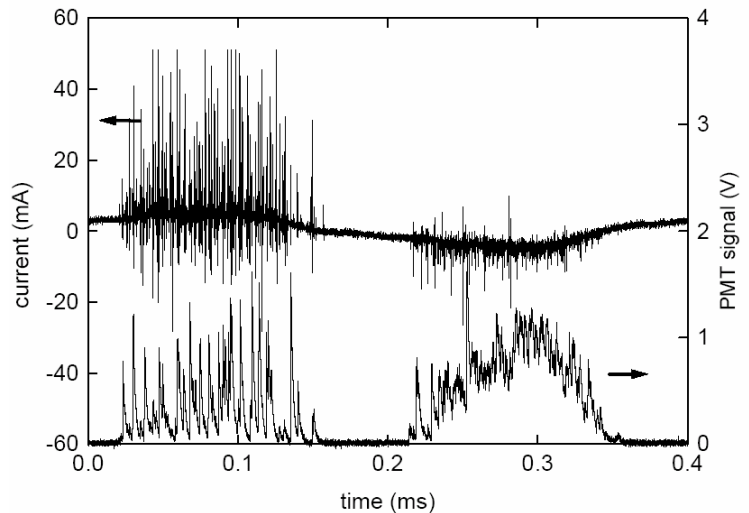


Figure 2. Current and light emission (PMT signal) from plasma actuator discharge. Reproduced from Ref. 6.

II. Computational Model

Simulation of the plasma was accomplished using a particle-in-cell direct-simulation-monte-carlo (PIC-DSMC) method. It has been exhaustively documented in the literature¹²⁻¹⁷ and will be only briefly discussed here. In the particle-in-cell method, a single computational particle represents thousands or millions of charged particles of one species (ion or electron). The particle motion is updated in time as influenced by the forces due to the electric fields. The electric fields are calculated by differentiating the electric potential which is computed by solving the Poisson's equation. The charge distribution for the solution of the Poisson's equation is determined from the particle positions. A plasma is characterized by following the behavior of thousands or millions of computational particles. At each time step, the force is calculated on each particle from the local electric fields. The velocities are then updated from the forces and new particle positions are computed using a leap-frog method.¹² A new charge distribution is, then, determined from the updated particle positions and the electric potential and resulting electric fields are computed from the new charge distribution. The method is repeated at each time step. In the present simulation, both ions and electrons are treated as computational particles.

The plasma actuator operates at atmospheric pressure. Due to the high air density, the collisions between the plasma particles and the neutral (air) molecules can not be ignored. For this reason, a Monte-Carlo^{16,17} method was used to evaluate the collision events. A no-time-counter method¹⁶ is utilized during each time step to determine which ions and electrons have collided with the air molecules. Any chemistry which may take place due to the collision is also evaluated. Any momentum transfer is recorded and any chemical change due to a collisional event is used to update the concentration of species in the cell. Because the electron avalanche takes place in 10's of nanoseconds the neutrals do not have sufficient time to move any significant distance. Therefore, the neutrals are treated as a background component of the simulation and their motion is not modeled.

The simulation is conducted in pure nitrogen. The oxygen in the air is thought to significantly alter the discharge due to the presence of negative (O-) ions. This leads to different ion recombination behavior, altered sheath structure, and perhaps, even different force production characteristics. In the interest of understanding the physics of the discharge, however, the simpler case of pure nitrogen is examined in the present study. The addition of oxygen and its associated chemistry will be made in future studies.

The chemical reactions allowed in the present study are shown in Table 1. They include electron momentum transfer, molecular ionization, excitation, and dissociation. It also includes nitrogen molecule momentum transfer and charge exchange. These last two reactions will be the primary mechanism for momentum transfer (force) to the neutrals. Electron momentum transfer is important in correctly calculating the energy of the electrons but does not significantly affect momentum transfer to the neutrals. No rate constants were used in calculating the reactions. Instead, the collision cross sections from ref. 18 were used directly to determine the probability of any collision event taking place.

Table 1. Chemical Reactions in the Simulation

e	$+$	N_2	\rightarrow	N_2	$+$	e	momentum transfer
e	$+$	N_2	\rightarrow	N_2^+	$+$	$2e$	ionization
e	$+$	N_2	\rightarrow	N_2^*	$+$	e	excitation
e	$+$	N_2	\rightarrow	$2N$	$+$	e	dissociation
N_2^+	$+$	N_2	\rightarrow	N_2^+	$+$	N_2	momentum transfer
N_2^+	$+$	N_2	\rightarrow	N_2	$+$	N_2^+	charge exchange

The computational geometry is shown in Fig. 3. It consists of two electrodes separated by a dielectric. The upper electrode is 0.5 mm thick and protrudes only 0.25 mm into the computational domain. Initially a larger exposed electrode was utilized, but the plasma was found not to exist significantly beyond the right edge of the electrode. For this reason, the exposed electrode was shortened. The buried electrode is 1.25 mm long and is a boundary condition below the dielectric. The dielectric is 0.5 mm thick. The computational domain is 1.5 mm high by 2.0 mm long by 0.1 mm wide.

The grid is 165 x 320 cells. In the plasma region, the cells are 6.25×10^{-6} m square (height and length) by 0.1 mm wide. Only every fourth cell in the plasma region is shown in the figure for clarity. The electrode and dielectric thicknesses are chosen to be representative of the experimental setups currently under investigation. The length of the buried electrode was shortened to decrease the computational work load. Longer electrodes can be used but were found unnecessary in the exploration of the discharge characteristics and force production mechanisms. The computational domain is one cell wide with reflective boundary conditions on either side. Therefore, although all particle motions and collisions are calculated in 3 dimensions, this is effectively only a 2 dimensional simulation. Because the experimental electrodes are long and slender, however, the plasma is 2 dimensional to a good approximation.

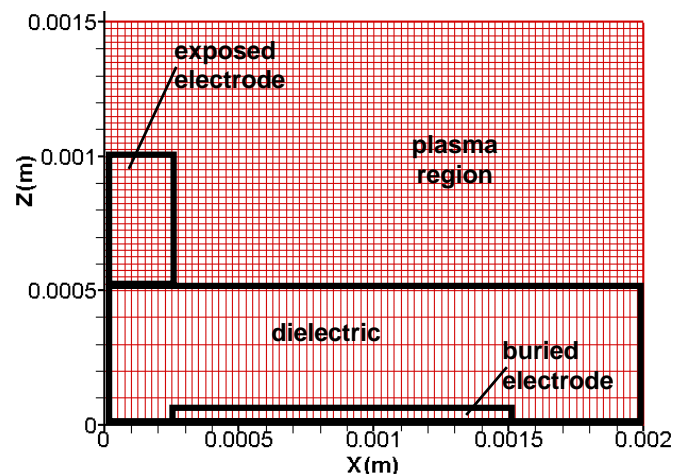


Figure 3. Computational geometry.

Particle boundary conditions were as follows: Particles exiting the computational domain were deleted from the computation. Particles striking the exposed electrode would be neutralized and, therefore, were also deleted from the simulation. Particles striking the dielectric were held at the dielectric boundary and their velocity was set to zero. In the actual plasma, an electron or an ion may bury itself into the dielectric due to the impact momentum. This may affect the speed at which the particles leave the dielectric when the electric field reverses since some energy has to be expended to extract them from the surface. It would also affect the timing of their departure since the electric field has to rise above some threshold for extraction. No attempt to model this has yet been made in the current simulation.

Electrical boundary conditions were as follows: The potential gradient was set to zero along the plasma boundaries. The potential was computed by solving the Poisson's equation throughout the domain, including the dielectric. The dielectric constant is currently set to 1.0. The buried electrode was held at zero Volts, while the exposed electrode was held at either 5000 V or -5000 V. A time varying potential was attempted, but since the electron avalanche takes only $10\text{-}20 \times 10^{-9}$ sec and the collision frequency with the neutrals forces a time step of about 1×10^{-15} sec, attempting to capture a single bias cycle is prohibitively expensive. Instead, the potential of the exposed electrode was set to -5000 V and the discharge was computed until it extinguished. This was followed by setting the potential to 5000 V and, again, computing the discharge until it extinguishes. Therefore, the simulation utilizes a square wave input to the electrodes.

Different grid densities were tried for the simulation. The cell size in the plasma region was reduced from 2.5×10^{-5} m to 0.4×10^{-5} m until the force began to converge. Further reductions were not made due to computational constraints.

The simulations were started by seeding the flow with a small number of electrons. Trials were conducted where the number of seed electrons was reduced until the discharge became independent of the size of the seed. This is a standard technique in this type of simulation.^{14,15} The seed electrons are placed near the upper corner of the exposed electrode where secondary electron emission is expected. The plasma discharge then evolves self-consistently as the electrons accelerate in the electric field and cause further ionization, dissociation, etc.

III. Computational Results

Simulations were conducted of a 2-dimensional slice of a dielectric barrier discharge at atmospheric pressure and density with a square wave input of amplitude 5000 V. The bias cycle frequency is not specified but is low enough to allow the discharge to extinguish before it reverses polarity. In the present simulation, this results in an effective frequency in the 1-10 mega-Hertz range.

The initial electric potential and electric field vectors are shown in Fig. 4. As expected, the potential contours are widely spaced away from the electrodes and show a large gradient where the electrodes are closest to each other. Generally, the electric field points from the buried electrode to the exposed electrode. The vector lengths are proportional to the electric field magnitude. The maximum field magnitude is about 7.3×10^6 V/m and it occurs near the lower edge of the exposed electrode. At the right edge of the computational domain, the field strength is only about 1.0×10^6 V/m. The contours are continuous across the dielectric/vacuum interface due to the present choice of the dielectric constant.

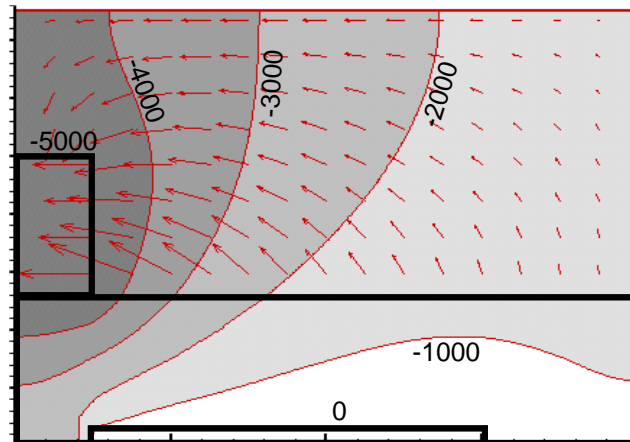


Figure 4. Electric potential (V) and electric field vectors at $t = 0.0$ sec.

A. Initial Plasma Discharge - Forward Stroke

The charged particle density throughout the first 30 nsec is shown in Fig. 5. The electrons accelerate along the electric field lines (tangent to the field vectors) and cause further ionizations as they stream toward the buried electrode. Note that the head of the avalanche is predominantly electrons, while the tail is predominantly ions. This occurs because of the high ambient neutral density. The ions, suffering numerous collisions with the neutrals, are halted from following the head of the streamer. The high energy electrons continue forward while the low energy electrons remain with the ions. Such behavior has been observed before¹⁹⁻²² and is typical of the Townsend phase of the streamer discharge. The energetic electrons stop their progress when they collide with the dielectric covering the buried electrode. In the figure this is indicated with the large negative charge density contours in the dielectric.

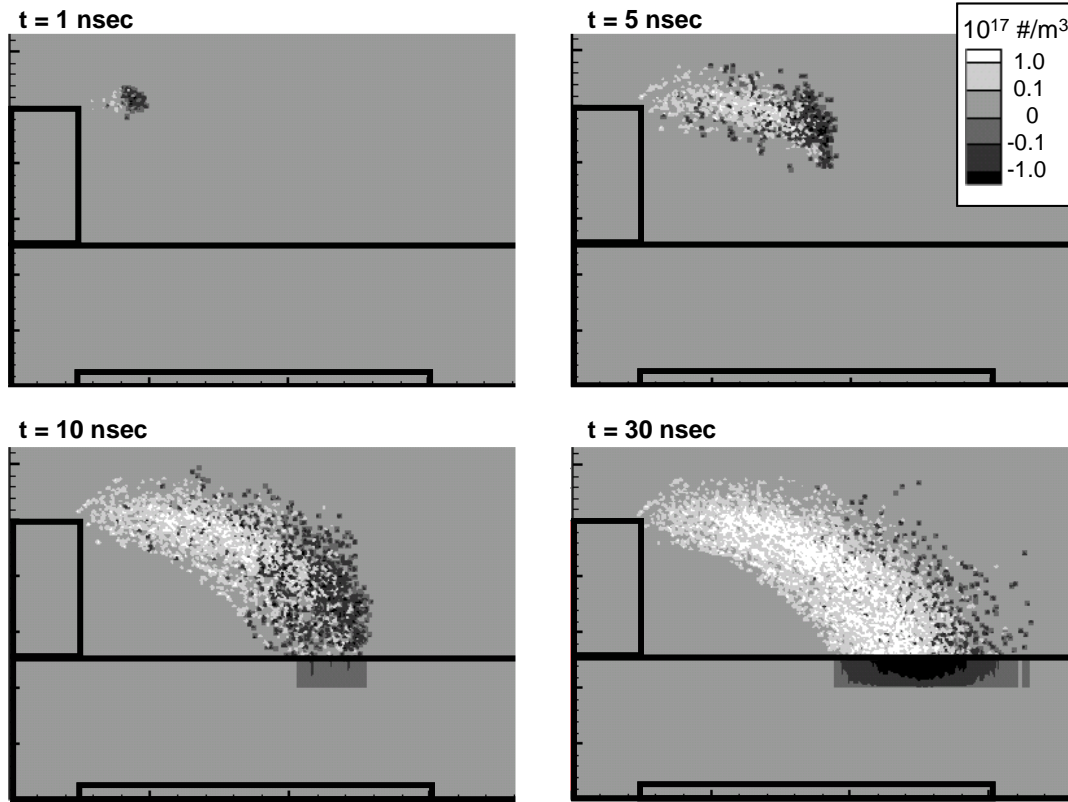


Figure 5. Charge density contours during forward stroke.

When sufficient electrons strike the dielectric, the local vertical electric field is diminished. This results in subsequent electrons landing further away from the exposed electrode (to the right in the figure). Continuing the simulation forward in time from this point does not produce significant further ionization, dissociation, or excitation, since most of the electrons are now resting on the dielectric. These electrons, therefore, no longer accelerate, gain energy, or collide with neutrals. In the experiment, light emissions would cease after this time because the nitrogen meta-stable lifetime is on the order of tens of microseconds at these pressure and density.²³ Therefore, the glow may persist after the ions and electrons are recombined. The lack of further ionization is clearly shown in Fig. 6 which displays the total number of computational particles (ions and electrons) as a function of time. New ionization events cease after about 30 nsec.

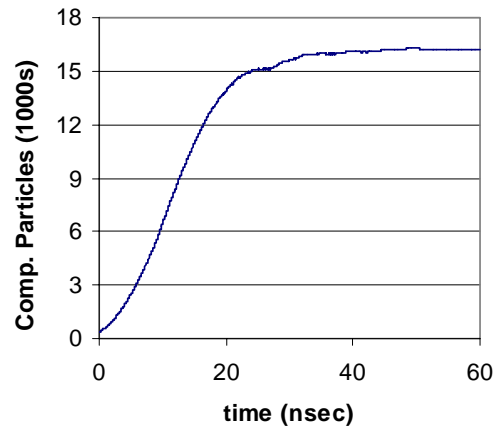


Figure 6. Computational particles during forward stroke. Ionization events stop after about 30 nsec.

In addition to ionization, the electrons accelerating in the electric field also produced dissociation and excitation of the molecular nitrogen. Figure 7 displays the atomic nitrogen density contours which result from dissociation collisions at time = 30 nsec. The atomic nitrogen contours follow the path of the discharge producing an area with a density of about 10^{17} #/m³. Also left in the wake of the discharge are large amounts of excited molecular nitrogen, shown in Fig. 8 for the same time in the discharge. The light emission from the plasma observed in the experiments is most closely associated with this species since it will release a photon when it de-excites.

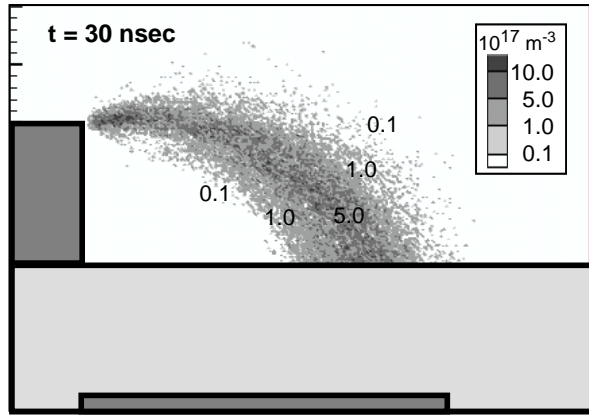


Figure 7. Dissociated nitrogen (N) density contours during forward stroke.

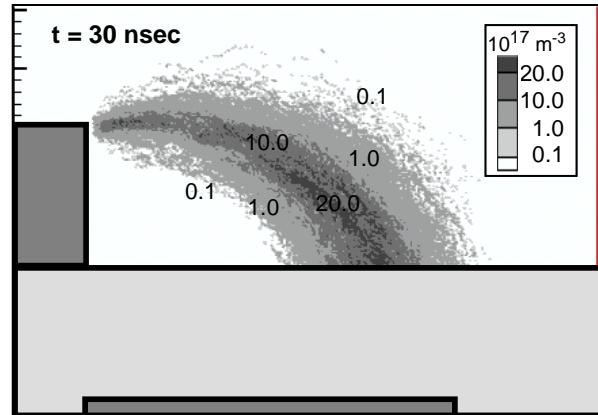


Figure 8. Excited nitrogen (N₂*) density contours during forward stroke.

B. Reverse Plasma Discharge – Back Stroke

At time = 60 nsec the electrode bias was reversed and computations were continued for another 60 nsec. This gives an effective frequency of about 8×10^6 Hz. This is much larger than in the experiments, but it is still useful in shedding light on the nature of the plasma discharge. The important similarity maintained between the experiments and the computations is that for both, the ionization events have effectively ceased before the field reverses.

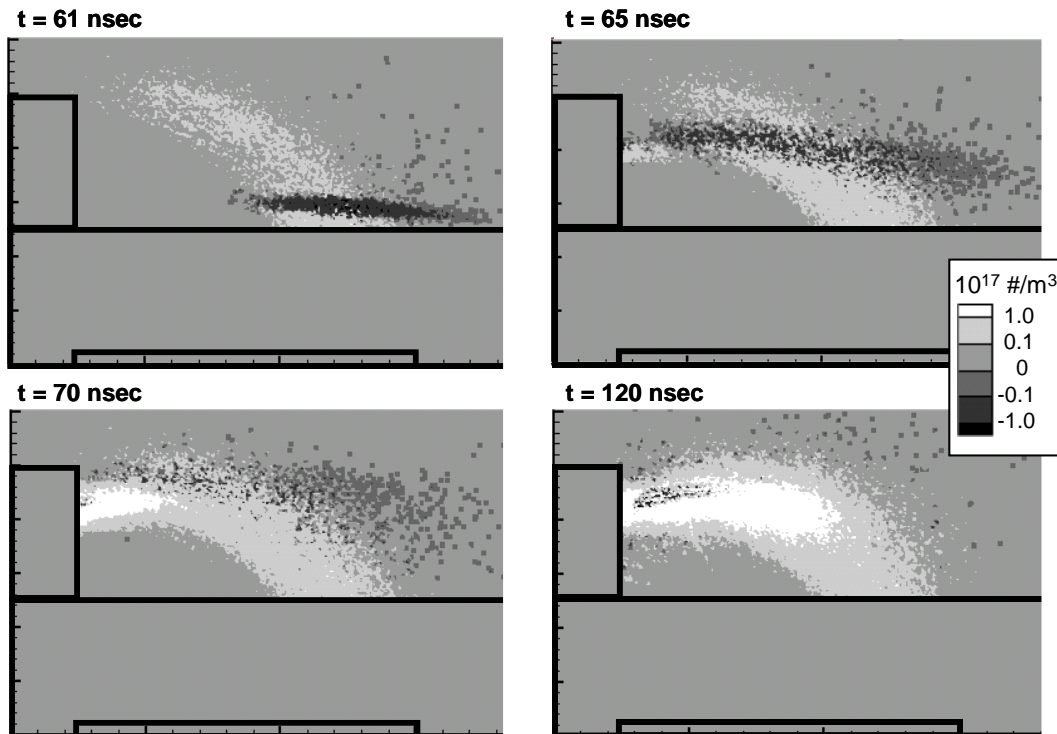


Figure 9. Charge density contours during back stroke.

As soon as the electric field is reversed the electrons which have been resting up against the dielectric during the forward stroke, start to accelerate back toward the exposed electrode and begin to again ionize, dissociate, and excite the molecular nitrogen. The charge density contours for the back stroke or second half of the bias cycle is shown in Fig. 9 for various points in time. The electrons leave the dielectric (the dark cloud in the figure) and begin moving toward the exposed electrode. The ions, because the exposed electrode is at 5000 V during the second half of the bias cycle, will now be pushed toward the dielectric. By $t = 65$ nsec, some electrons have already hit the exposed electrode and left the plasma (due to neutralization). The ion density has risen from an average of 1×10^{17} to 5×10^{17} $\#/m^3$. Five nanoseconds later (at $t = 70$ nsec), the bulk of the electrons have reached the exposed electrode and the ion density contours peak at 1×10^{18} $\#/m^3$. At $t = 120$ nsec the peak ion density is above 3×10^{18} $\#/m^3$. The time average ion density over the entire computational domain is 6×10^{16} $\#/m^3$ (due to large regions without any ions). During the forward stroke, however, the time average ion density is only 4×10^{15} $\#/m^3$. The results, therefore, show that the average ion density during the back stroke is at least 10 times higher than the average ion density during the forward stroke. This is important because it is the ions which will be responsible for gaining momentum from the electric field force and imparting it to the ambient neutral flow.

Ionization in the forward stroke was largely over in the first 30 nsec. In the back stroke, however, ionization had not halted after 60 nsec ($t = 120$ nsec). This is illustrated in Fig. 10 which shows the number of computational particles as a function of time. Through out the entire half of the bias cycle, the amount of particles continued to grow, although, the majority of the ionization occurs in the first 30 nsec.

The extended period of ionization during the back stroke may be caused by a combination of factors. The plasma charge density during the back stroke is sufficiently large to change the global potential distribution and electric fields, shown in Fig. 11. The maximum electric field above the dielectric during the back stroke is about 5.5×10^6 V/m, where as, during the forward stroke the maximum electric field was 7.3×10^6 V/m. This could translate to smaller electron acceleration which would take longer to reach energies capable of ionization. In addition, the back stroke is starting its avalanche with a vastly larger number of electrons. This alone will lead to a larger amount of ionization.

The difference in the length of the ionization periods between the forward and the back strokes may suggest a way to make the method more efficient. If the back stroke leads to greater ion densities and longer periods of ionization, it may be advantageous to choose a bias cycle profile where the back stroke is longer than the forward stroke. For example: the time during which the potential of the exposed electrode is positive could be made longer than the time during which it is negative.

The density contours, at $t = 120$ nsec, for dissociated (atomic) nitrogen and excited nitrogen are shown in Figures 12 and 13, respectively. The atomic nitrogen (N) density levels have soared to above 1×10^{19} $\#/m^3$. This magnitude is a factor of 10 higher than the atomic nitrogen magnitudes on the forward stroke of the discharge. The excited nitrogen levels are also a factor of 10 higher than the levels during the forward stroke. Comparing Figures 13 and 8 reveal a curious behavior which has also been experimentally observed. The plasma glow is observed⁶ farther from the exposed electrode on the back stroke than

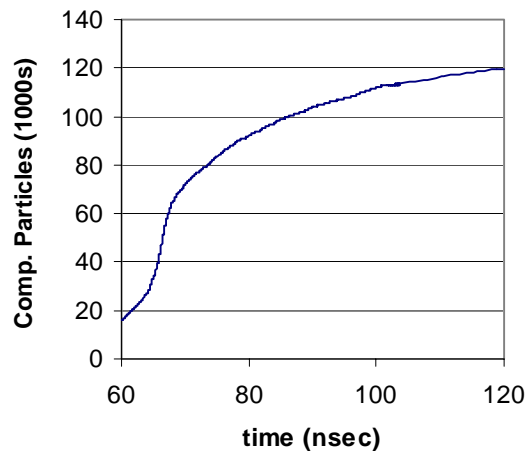


Figure 10. Computational particles during back stroke. Ionization events have not halted after 120 nsec.

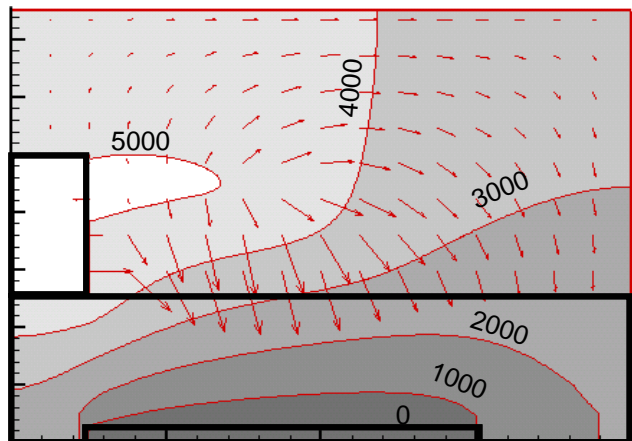


Figure 11. Electric potential (V) and electric field vectors at $t = 120.0$ sec.

on the forward stroke. Simulations show the same behavior, when excited nitrogen is considered as the species responsible for emission. Figure 8 showed that the excited nitrogen reached the end of the buried electrode during the forward stroke. Figure 13 shows that, during the back stroke, the excited nitrogen reaches significantly beyond the end of the buried electrode. This behavior may be due to several reasons: Electrons landing beyond the end of the electrode may have been repelled and, therefore, decelerated by the electrons already on the dielectric. This would leave them with insufficient energy to cause further nitrogen excitation. Alternatively, electrons landing beyond the buried electrode may simply have been born and landed on the dielectric before having a sufficient time to gain energy and cause molecular excitation. In either case, when the electric field reverses during the back stroke, these electrons, which landed beyond the buried electrode, accelerate and gain sufficient energy to cause excitation and plasma light emission from a larger region.

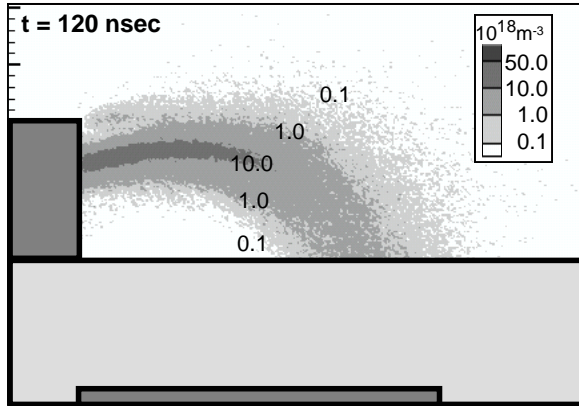


Figure 12. Dissociated nitrogen (N) density contours during back stroke.

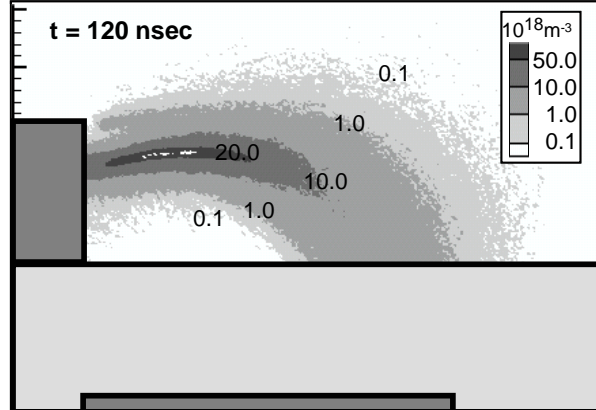


Figure 13. Excited nitrogen (N_2^*) density contours during back stroke.

C. Force Production Mechanism

In the previous sections, the charged particle densities and the plasma products were discussed. It was noted that the ion density was a factor of 10 higher during the back stroke than during the forward stroke. In this section, the significance of this asymmetry to the force production will be explored.

Figure 14 shows the vectors of force imparted by the ions to the neutrals at $t = 60$ nsec. Note that, although the electron avalanche during the forward stroke is toward the buried electrode, the force imparted to the nitrogen is toward the exposed electrode. This occurs because the ions are forced toward the exposed electrode by the -5000 V bias and the resulting electric field. Averaging the force in the x direction on the neutrals over the entire domain during the forward stroke results in a net force of -0.2×10^{-6} N. This force is, as the vectors indicate, toward the exposed electrode.

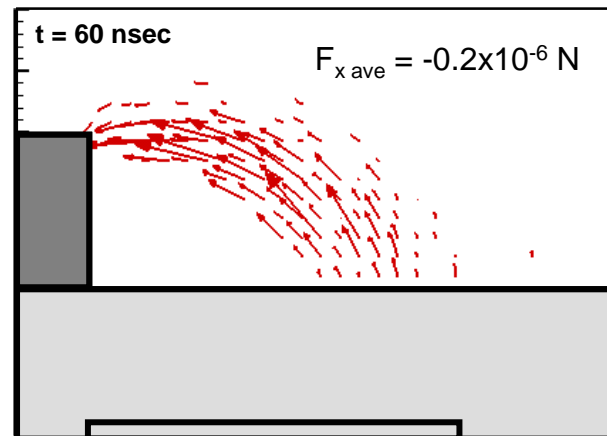


Figure 14. Vectors of momentum transfer to the neutrals at the end of the forward stroke.

Figure 15 shows the vectors of force imparted by the ions to the neutrals at $t = 120$ nsec. During the back stroke, the electrons avalanche toward the exposed electrode but the ions are pulled toward the buried electrode by the electric field. The net force on the neutrals, therefore, is directed toward the buried

electrode. The average force in the x direction over the domain and during the entire back stroke is 1.4×10^{-6} N. This is 7 times greater and in the opposite direction than during the forward stroke. The force is greater during the back stroke because of the disproportionately larger ion density.

Averaging the force over the entire electrode bias cycle (forward and back strokes) gives a net force of 6.0×10^{-7} N in the direction of the buried electrode. Therefore, the plasma actuator appears to produce a net force away from the exposed electrode and toward the buried electrode because of the larger production of ions during the second half of the bias cycle.

In order to make a sanity check, the force will be compared to a similar experiment. The current simulation results are generated with a power utilization of about 20 W. Ref. 6 reports a force of 0.0013 – 0.0020 N for a plasma actuator operating at 20 W. The experimental actuator was 250 mm wide (dimension into the page on Fig. 3). Since the simulations represent a 2-D slice which is only 0.1 mm wide, the total computational force for an actuator with a width equal to the experimental actuator would be 0.0015N. Therefore, the computations appear to be in the correct neighborhood. This serves as a sanity check only, since the simulations do not include the oxygen negative ion chemistry present in the air and the bias frequencies do not match. Never-the-less, this gives confidence to the results of the simulations.

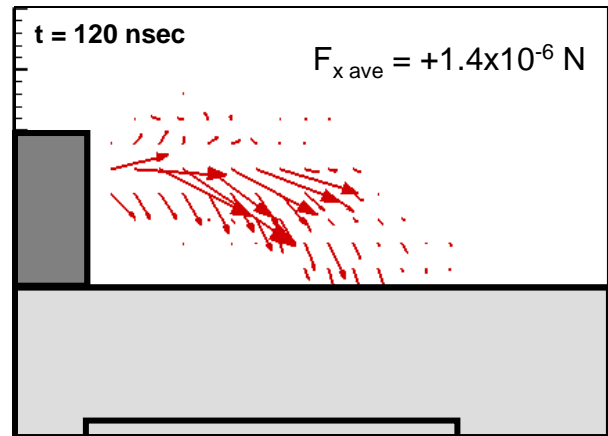


Figure 15. Vectors of momentum transfer to the neutrals at the end of the back stroke.

These computations were carried out over a single electrode bias cycle only. However, since the plasma is extinguished at the end of each half of the bias cycle, the simulations should be representative of the physics occurring during all bias cycles. At the beginning of each cycle (during the forward stroke), the avalanche is begun with very few electrons present. The subsequent avalanche toward the buried electrode produces many electrons which halt their motion at the dielectric. The second half of the bias cycle (the back stroke), begins with all of the electrons produced during the forward cycle present. Therefore, the ionization will always be greater during the back stroke. At the end of the back stroke, almost all of the electrons enter the exposed electrode leaving the next bias cycle to begin, again, with relatively few electrons. The larger ion density during the back stroke will always produce a net force away from the exposed electrode and toward the buried electrode because that is the direction of the force on the ions. If both electrodes were covered with a dielectric, the forward and back avalanches would be symmetric and the net force should be zero. This, in fact, was tried in experiments carried out in Ref. 6. The authors report that, when both electrodes were covered by a dielectric, the force was not measurable. Smoke flow showed that some force, apparently smaller than the accuracy of the experimental apparatus, still forced the air in one direction. Therefore, some component of the force may still be due to the electric field gradient or some, as of yet, unexplored mechanism.

IV. Summary

Plasma actuators have demonstrated the ability to promote attachment of the flow around airfoils by providing momentum to the boundary layers. The method by which the momentum is imparted to the flow was the subject of the present study. A plasma actuator was simulated using PIC-DSMC methods at atmospheric pressure for a pure nitrogen flow. The electrodes were biased using a square wave function with a frequency of 8 MHz. Both the electrons and ions were modeled as computational particles. The electric field was determined self-consistently during each time step. Collisions were resolved with the neutrals allowing for ionization, dissociation, and metastable excitation. The results show that the actuator works as a dielectric barrier discharge, where the plasma is created through an electron avalanche. The ions gain momentum by accelerating in the electric field and, then, produce a force by transferring this momentum to the neutrals through collisions. Since the electric field reverses during the electrode bias cycle, the ions impart momentum in one direction during the first half of the cycle and in the opposite direction during the second half. The actuator produces a net force in one direction because the

avalanche is not symmetric during both halves of the bias cycle. All of the electrons produced during the first half of the bias cycle are still on the surface of the dielectric at the beginning of the second half of the cycle. This results in ionization during the second half of the cycle which is more than 10 times greater than that produced during the first half. The electrons generated during the second half of the cycle are eventually lost to the exposed (conducting) electrode. Therefore, the next bias cycle has to begin the process from scratch (with almost no electrons). The result is that the ion density during the second half of the cycle is always greater than during the first half. The force is, consequently, greater for the second half of the cycle. In this manner, the plasma actuator produces a net force which should always be directed away from the exposed electrode.

References

- ¹Roth, J. R., Sherman, D. M., and Wilkinson, S. P., "Boundary Layer Flow Control with a One Atmosphere Uniform Glow Discharge Surface Plasma," AIAA paper 98-0328.
- ²Hultgren, L. S., and Ashpis, D. E., "Demonstration of Separation Delay with Glow-Discharge Plasma Actuators," AIAA Paper 2003-1025.
- ³Huang, J., Corke, T. and Thomas, F., "Plasma Actuator for Separation Control of Low Pressure Turbine Blades," AIAA Paper 2003-1027.
- ⁴Post, M. and Corke, T., "Separation Control on High Angle of Attack Airfoil Using Plasma Actuators," AIAA Paper 2003-1024.
- ⁵Enloe, C. L., McLaughlin, T. E., Van Dyken, R., Kachner, K. D., Jumper, E. J., Corke, T. C., Post, M., and Haddad, O., "Mechanisms and Responses of a Single Dielectric Barrier Plasma Actuator: Geometric Effects," *AIAA Journal*, Vol. 42, No. 3, 2004, pp. 595.
- ⁶Enloe, C. L., McLaughlin, T. E., Van Dyken, R., Kachner, K. D., Jumper, E. J., and Corke, T. C., "Mechanisms and Responses of a Single Dielectric Barrier Plasma Actuator: Plasma Morphology", *AIAA Journal*, Vol. 42, No. 3, 2004, pp. 589.
- ⁷Lieberman, M.A., and Lichtenberg, A. J., *Principles of Plasma Discharges and Materials Processing*, Wiley, New York, 1994, Chaps. 1,11.
- ⁸Sankaranarayanan, R., Pashaie, B., and Dhali, S. K., "Characteristics of a Barrier Discharge in Monatomic and Molecular Gases", *Applied Phys Let.*, Vol. 74, No. 21, 1999, pp.3119.
- ⁹Kang, W. S., Kim, Y., and Hong, S. H., "Spatio-temporal Images of Single Streamer Propagation in Dielectric Barrier Discharge," *IEEE Trans Plasma Sci.*, Vol. 30, No. 1, 2002, pp.166.
- ¹⁰Liu, S. and Neiger, M., "Excitation of Dielectric Barrier Discharges by Unipolar Submicrosecond Square Pulses," *J. Phys. D*, Vol. 34, 2001, pp.1632.
- ¹¹Gibalov, V. I., and Pietsch, G. J., "The Development of Dielectric Barrier Discharges in Gas Gaps and on Surfaces," *J. Phys. D*, Vol. 33, 2000, pp.2618.
- ¹²Birdsall, C. K., and Langdon, A. B., *Plasma Physics via Computer Simulation*, Adam Hilger, Bristol, 1991, Chap. 9.
- ¹³Kunhardt, E. E., and Tzeng, Y., "Role of Electron-molecule Angular Scattering in Shaping the Electron-velocity Distribution," *Phys Rev. A*, Vol. 34, No. 3, 1986, pp.2158.
- ¹⁴Kunhardt, E. E., and Tzeng, Y., "Development of an Electron Avalanche and its Transition into Streamers," *Phys Rev. A*, Vol. 38, No. 3, 1988, pp.1410.
- ¹⁵Li, J., and Dhali, K., "Simulation of Microdischarges in a Dielectric-barrier Discharge", *J. Appl. Phys.*, Vol. 82, No. 9, 1997, pp. 4205.
- ¹⁶Font, G. I., and Boyd, I. D., "DSMC-PIC Simulation of a Helicon Etch Reactor and Comparison with Experiments," *Process Control, Diagnostics, and Modeling in Semiconductor Manufacturing*, Electrochemical Society, 1997, pp.275.
- ¹⁷VanGilder, D. B., Font, G. I., and Boyd, I. D., "Hybrid Monte Carlo Particle-in-Cell Simulation of an Ion Thruster Plume," *Journal of Propulsion and Power*, Vol. 15, No. 4, 1999, pp.530.
- ¹⁸Phelps, A. V., and Pichford, L. C., "Anisotropic Scattering of Electrons by N₂ and its Effects on Electron Transport," JILA Information Center Report No. 26, University of Colorado, 1985, *Phys Rev A*, Vol. 31, 1985, pp. 2932.
- ¹⁹Vitello, P. A., Penetrante, B. M., and Bardsley, J. N., "Simulation of negative-streamer dynamics in nitrogen," *Phys. Rev. E*, Vol. 49, No. 6, 1994, pp. 5574.
- ²⁰Braun, D., Gibalov, V., and Pietsch, G., "Two-dimensional Modeling of the Dielectric Barrier Discharge in Air," *Plasma Sources Sci. Tech.*, Vol. 1, 1992, pp. 166.
- ²¹Gibalov, V., and Pietsch, G., "The Development of Dielectric Barrier Discharges in Gas Gaps and on Surfaces," *J. Phys. D*, Vol. 33, 2000, pp. 2618.
- ²²Massines, F., Rabedhi, A., Decomps, P., Ben Gadri, R., Segur, P., and Mayoux, C., " Experimental and theoretical Study of a Glow Discharge at Atmospheric Pressure Controlled by Dielectric Barrier," *J. Appl. Phys.*, Vol. 83, No. 6, 1998, pp.2950.
- ²³Ekey, R. C., and McCormack, E. F., "A Planar Jet Expansion Discharge Source of Molecular Afterglow Emission," *Chem Phys Let*, Vol. 381, No. 3, 2003, pp. 416.